이학석사 학위논문

Terahertz transmission of PEDOT:PSS on nano slot antennas

나노 슬 랏 안테나 위 PEDOT:PSS 의 테라헤르츠 투과

2019 년 2 월

서울대학교 대학원

물리천문학부

오 승 인

Terahertz transmission of PEDOT:PSS on nano slot antennas

지도 교수 김 대 식

이 논문을 이학석사 학위논문으로 제출함

2019 년 **2** 월

서울대학교 대학원

물리천문학부

오 승 인

오승인의 이학석사 학위논문을 인준함

2019 년 **2** 월

위 원 장	이 탁 희	(인)
부 위 원 장	김 대 식	(인)
위 원	전 헌 수	(인)

Abstract

Poly(3,4-ethylenedioxythiophene)/poly(4-styrenesulfonate) (PEDOT:PSS) has actively been studied and used for its application in optical and electrical devices such as photovoltaic, solar cells and sensors due to its superb processibility, thermal stability, organic compatibility and high electric conductivity. In this thesis, PEDOT:PSS aqueous solutions with different dilution were drop casted on the slot antennas of which width ranges from micro to nano size and THz transmission was measured. PEDOT:PSS allows the flow of electric current across the antenna gap alleviating the capacitive charge accumulation and consequently leading to the decrease in transmission. Although the conductivity of PEDOT:PSS is 5 orders less than the ones of metal, the effect of PEDOT:PSS in transmission decrease appeared clearly favored by the strong electric field inside gap. The drop-cast of extremely diluted PEDOT:PSS solution of 0.001 wt.% which corresponds to a nano thin film displays transmission decrease of 19 % and 5.7 % in each case of 30 nm and 1 um slot antenna. The result implies that thin film of PEDOT:PSS on the nano slot can be applied as a real-time gas sensor with enhanced sensitivity.

Keywords : Terahertz Transmission, PEDOT:PSS, Nano-slot antenna

Student Number : 2017-22335

Table of Contents

1. Introduction

Since the discovery of extraordinary transmission through thin metal films perforated with an array of sub-wavelength apertures, the newly introduced concept for the enhanced transmission, surface plasmon polariton (SPP), has been investigated extensively for decades. (1) In the visible and near-infrared regions, the enhanced transmission of light in metallic structures can be achieved by the surface plasmon response. (2, 3, 4) In the terahertz regime, the coupling between electromagnetic waves and moving charges at the metal surface is typically weak for the planar metal. However, as the waveguide cross-section tends to be a nanoscale, high electric field confinement appears at THz frequencies. (5) It was shown that the nanogap width which was approximately four orders of magnitude smaller than the incident wavelengths exhibited enormous field enhancement of a thousand. (6) The tight confinement of high intensity THz field into small spatial areas provides various potential applications such as nonlinear optics, deep-subwavelength imaging and sensing.

Among many applications of metamaterials based on nano scale gap structures, devices for chemical and biological sensing have been developed actively exhibiting enhanced THz absorption cross section by virtue of field enhancement. (7, 8, 9) Recently, along with colossal THz absorption, it is implied that utilization of charge transfer across the metal gap due to field enhancement leads to THz applications with advances. (10) Besides light absorption mechanism, charge transfer mechanism can solely or mainly be utilized in metamaterial applications. Applications of conductive polymers on

the gap of metamaterials have been researched recently. For example, real-time gas sensor based on split ring resonator coupled with conducting polymer (11) and terahertz metamaterials acting as transducers for chemical sensor (12) were reported recently.

In this thesis, the effect of conductive polymer on transmission amplitude decrease in THz transmission of metamaterial is investigated. Here we choose slot antennas as metamaterials and aqueous PEDOT:PSS solution was drop casted on slot antennas to form conductive polymer across metal gap. To see the effect of conductive polymer on the transmission with different field enhancement, 1 um and 30 nm were chosen for the width of slot. Since now the metal gap is filled with conductive material, the following questions arise naturally. Will the THz wave-induced charge accumulation of electrons on the capacitive metal gap be alleviated enough by the current across the metal gap bridged by the conductive polymer even though the electronic conductivity value of metal is significantly higher (5 orders) than the one of PEDOT:PSS? How much small amount of PEDOT:PSS can be placed on the metal gap so that there is a recognizable decrease in transmission? To answer these questions, water-diluted PEDOT:PSS solutions with various concentration were drop casted on gold slot antennas. Slot width was varied from micro scales to nano scales.

2. THz transmission of Nano slot antennas

One of famous analytical approach for the strong resonance transmittance through a subwavelength rectangular hole was conducted by F. J. Garcia-Vidal et al.. (13) According to this theory, transmittance is controlled simply by lengths of two sides of rectangular. With the approximation of subwavelength regime and perfect electronic conductor (PEC) treatment on metal, the normalized-to-area transmission can be obtained by $T_{res} \approx \frac{3}{4\pi}\frac{{\lambda_{res}}^2}{a_x a_y} \approx \frac{3a_y}{\pi a_x}$, where a_x and a_y are length of short side and long side and λ_{res} is resonance of wavelength which is approximately two times of long side length. Since ratio of long side to short side of rectangular is proportional to the normalized-to-area transmittance at resonance, a huge transmittance can be obtained if aspect ratio of rectangular hole is high enough.

Other than short wavelength regimes such as UV and visible spectrum, PEC condition has been applied on metal in THz regime. The plasma frequency of metals is typically in the UV region of the electromagnetic spectrum. According to Drude model, the real and imaginary components of permittivity of metals have very large absolute values in terahertz regime. Thus it is valid that metal is treated as perfect electronic conductor (PEC) in THz regime and the aforementioned relations are applicable.

Using the fact that strong field enhancement can be occurred by narrowing the width of gap, a lot of researches has been conducted theoretically and experimentally. (6, 14, 15, 16)

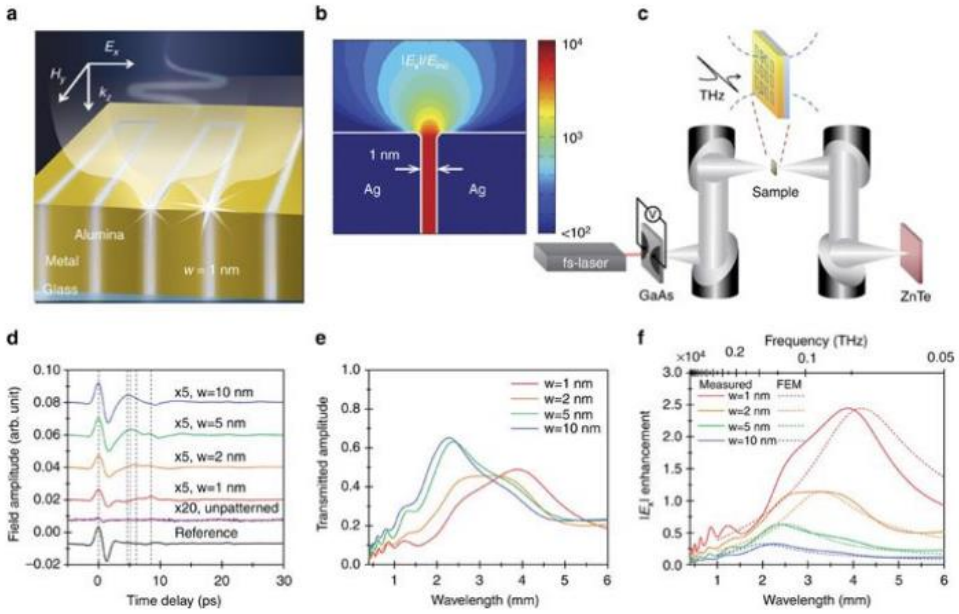

Figure 1 Giant THz field enhancements in nanogap ring structures (from Ref. 14)

Fig. 1 (a) is the illustration of THz waves being funneled through nanogaps. Fig. 1 (b) is a 2D FDTD simulation presenting electric-field enhancement reaching up to four orders of magnitude in the 1 nm-wide slit. Fig. 1 (c) shows experimental setup for THz-TDS. FIg. 1 (d) is time traces for transmitted THz waves through the bare substrate (reference), unpatterned Ag film and nanogap samples with the gap sizes of 1, 2, 5 and 10 nm. Fig. 1 (e) is Fourier-transformed electric-field transmitted amplitude, normalized by the reference signal, as a function of wavelength. In fig. 1 (f), field enhancement was plotted in frequency domain.

Dashed lines indicate calculated transmission spectra and solid lines indicate measured fields.

2.1. Transmission dependence on slot geometry

The incident light onto the slot induces the current in the metal surfaces accumulating near the edges of metals. Owing to this accumulation of charges, the enhanced electric field presents inside the nanogap. When the thickness of metal film h and gap width w are similar in size, the accumulations are spread slightly away from the edges by the gap size explaining the strong dependence of field enhancement on the gap size. The distortion of current flow on the metal surface can be alleviated and resemble the straight current flow on bare metal film when the size of width is smaller than that of thickness. In this case, we can get the ultimate field enhancement factor, $\frac{E_{gap}}{E_0} = \frac{\lambda}{(\varepsilon_{gap}\varepsilon_0)\pi h}$ which is independent of gap width. E_0 is the incident electric field amplitude and E_{gap} is the transmitted electric field amplitude through the apertures. ε_{gap} and ε_0 are permittivity of the gap material and vacuum respectively. (16)

Fig. 2 shows that the electric field enhances dramatically and resonance transmission is blue-shifted as the gap thickness decreases. (17)

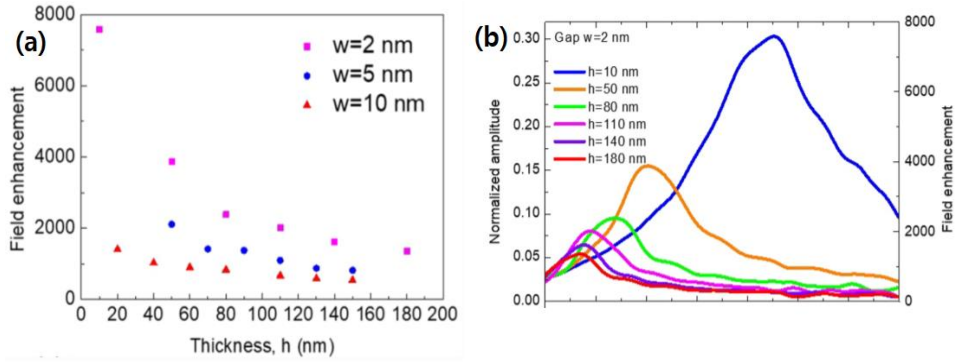

Figure 2 (a) Field enhancements of nano gap antennas as a function of the gap thickness (b) Experimental normlaized transmissions and field enhancements of 2 nm wide slots on quartz substrate (from Ref. 17)

As the gap width is reduced, metal surface plasmons coupling over the gap become considerable. Limit in field enhancement and red shift in resonance transmission come from gap plasmon. (18) As the gap width goes further to subnanoscale, a substantial decrease in transmission amplitude is observed. Electrons at the gap edge tunnel through the potential barrier of subnanogap preventing charge accumulation at the metal edges resulting in reduced field enhancement. (19) Recently it is reported that quantum tunneling of nano gap can occur over 1 nm-width gap regime. (20)

2.2. Transmission dependence on surrounding dielectric mediums

The transmission resonance of nano gap supported by substrate is red shifted compared by the free standing one. The resonance wavelength is related with n_{res} by $\frac{\lambda}{2} = n_{res} a_y$ where the refractive index n_{res} depends on gap thickness and lies in between 1 and the substrate refractive index. (21)

Besides resonance behavior, the substrate affect the field enhancement as shown in Fig 3.

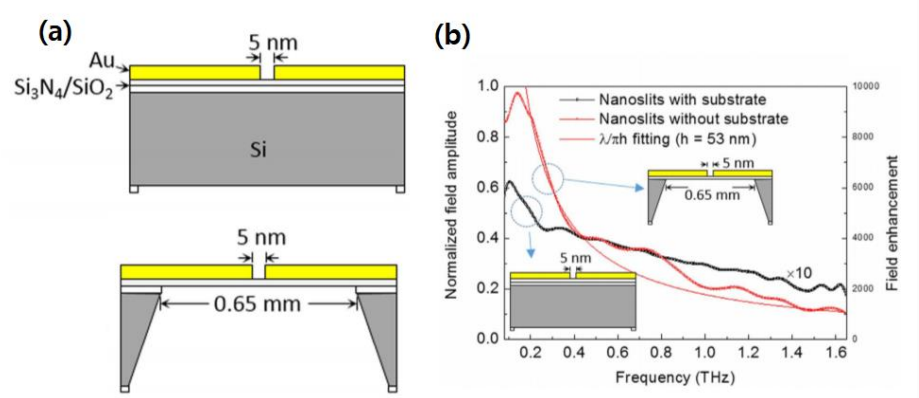

Figure 3 Transmission of 5-nm slits with/without silicon substrate (from Ref. 22)

Cross-section scheme of 5-nm slits with/without silicon substrate of 300 um thickness is depicted in Fig. 3 (a). 15 fold enhanced field enhancement is observed at 0.14 THz when Si substrate is removed. The reduced field enhancement with substrate can be explained by the nanoslit response to a effectively smaller wavelength $\lambda_{eff} = \frac{\lambda}{n_{eff}}$ where n_{eff} is given by

$n_{eff} = \sqrt{\frac{n_g{}^2 + n_s{}^2}{2}}$. n_g and n_s denote refractive index of gap and substrate respectively. (22, 23)

The peak position of field enhancement can also be affected by thin dielectric film coated on nano gap. (24) The resonance behavior has been investigated with sub-10 nm annular gap array. The 10 nm gap displays 3 times higher sensitivity than 1 um gap on detection of 10 nm aluminum oxide (Al2O3) film. Since the refractive index on the gap is replaced by the one of Al2O3 instead of air one, peak resonance behavior shows red-shift. However, sub-nano gap (2 nm, 5 nm) showed lower sensitivity with 10 nm dielectric overlayer. Stronger field confinement brings narrower probing region over the gap, which is related with field decay length. Gap-plasmon explains that as gap narrows, effective mode index becomes higher rendering the nano gap less sensitive to the index of overlayer.

2-3. Applications of nano slot antenna composites

As for a first example of the application of nano slot antenna, hybrid nanogap-VO_2 device exhibits an anomalous transition behavior with switching actions at much below the insulator to metal transition temperature of bare vanadium dioxide. (25)

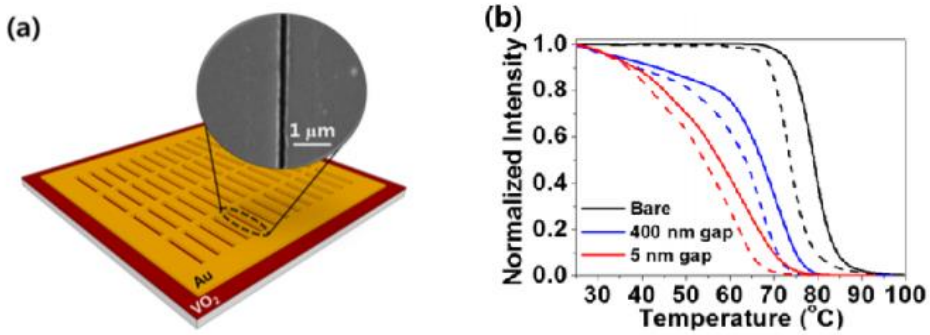

Figure 4 Anomalous transition behavior of hybrid nanogap-VO2 device (from Ref. 25)

Vanadium dioxide has temperature dependant phase transition from insulator to metal state at 68 °C. The hybrid structure is depicted in Fig. 4 (a). Gold is patterned on VO_2 film using conventional photolithography and atomic layer deposition method. At even 40 °C earlier than vanadium transition temperature, the responses of thermally excited electrons and holes are

considerable in terahertz transmission due to nano gap interaction as shown in Fig. 4 (b). This result implies a potential application as a room-temperature phase transition device.

In a second example, tens of nanograms of RDX (1,3,5-trinitroperhydro-1,3,5-triazine) drop casting on a single nano slot was conducted filling the gap with only tens of femtograms of molecules. (7)

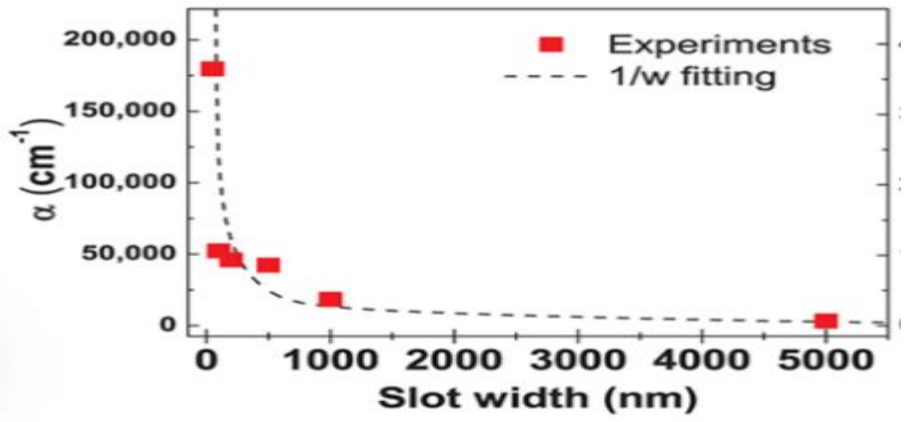

Figure 5 Absorption coefficient of molecules filling the gap as function of slot width (from Ref. 7)

The colossal absorption coefficient of nano slot antenna can reach over the value of $100000\ cm^{-1}$ with three orders of magnitude of cross section of the molecules as illustrated in fig. 5. In nano slot environment, the asymmetric electromagnetic ratio, $\frac{E}{Z_0 H}$ over 103, is the main mechanism of colossal absorption. Here E and H are respectively electric and magnetic field inside nano

slot and Z_0 is impedance of free space. This is promising working frame in THz chemical and biological sensing area.

As empirically shown in above examples, the small change of gap material's property brings abrupt changes of optical signals in THz regime.

3. PEDOT:PSS

A conductive polymer, poly(3,4-ethylenedioxythiophene):poly(styrene sulfonate) (PEDOT:PSS), consists of PEDOT and PSS. PEDOT is a conjugated polymer and carries positive charges. PSS carries negative charges and is deprotonated polymer surfactant which helps stabilize PEDOT in water and other solvents. PEDOT:PSS dispersed in water is shown in Fig. 6.

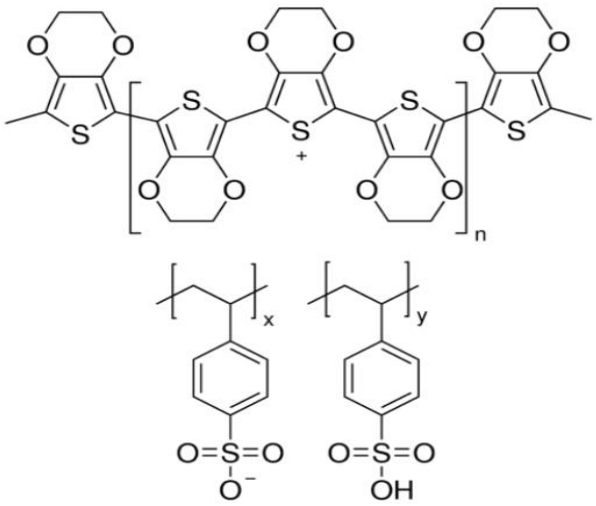

Figure 6 The chemical structure of PEDOT:PSS dispersed in water (Image from Sigma Aldrich Company)

PEDOT:PSS possesses great processability with water, high transparency in visible range, catalytic properties, mechanical flexibility, thermal stability and high conductivity (~1S/cm) among other polymers. A wide range of electrical conductivity from 10^{-2} to 10^{4} (S/cm) with additives or post treatment. (26,

27) Also, continuous thin film can be built on various substrates by spin coating, drop casting, doctor blade, spray deposition, etc.

The conductivity of PEDOT:PSS can be enhanced significantly with diverse strategies. For example, the treatment with organic solvents or ionic molecules enable the conductivity to reach up to 100 S/cm. (28, 29) Recently, a lot more improved conductivity enhancement has been achieved. Initial doping with dimethyl sulfoxide(DMSO) and adding LiClO4 as a secondary dopant provide the PEDOT:PSS film with the conductivity of 950 S/cm. (30) Treatment with organic solutions and salt of the organic solution, methylammoniun bromide (MAI), give the highest value of 2100 S/cm. (31)

As for the application, PEDOT:PSS can be applied as transparent electrode in organic solar cells device. Owing to its advantages such as good adhesion to organic and polymeric materials, low cost expense, flexibility and fast response, PEDOT:PSS has been accepted one of prominent future component in organic solar cells replacing indium tin oxide (ITO). (32, 33) Besides organic solar cells, a wide range of applications such as LED electrode, photovoltaics and field-effect transistor are included. (34, 35, 36)

4. Experiment

4-1. Fabrication of slot antennas

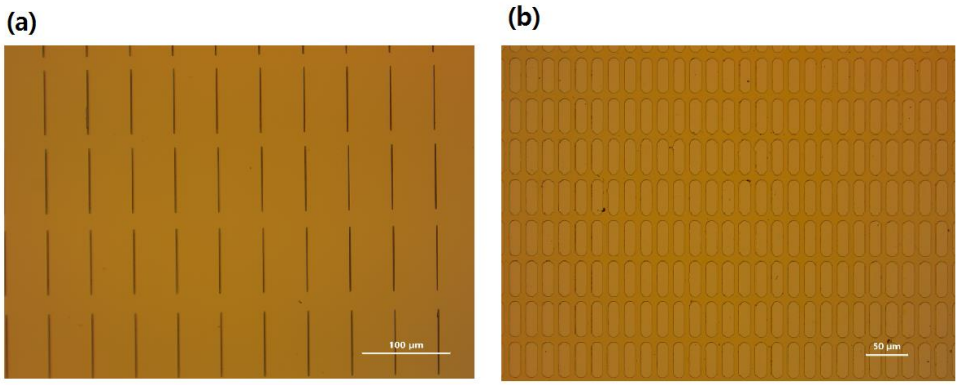

Figure 7 The microscope images of slot antennas

Negative photoresist (MAN 2405) was spin coated on silicon substrate of 500 um thickness and 1 cm by 1 cm area. After soft baking, photoresist was written by electron beam. After developing photoresist with a developer solution (ma-D 525), 100 nm thin gold film was deposited on silicon substrate using e-beam evaporator machine. We fabricated slot antenna of which length and width are 80 um and 1 um respectively. The 20 by 10 slot antennas were arranged over 1 mm by 1 mm area with 50um by 100 um periodicity. The microscope image of 1 um-width-slot antenna is displayed in Fig. 7 (a).

For the fabrication of rectangular shaped nano gap sample, we used conventional atomic layer lithography method. Photoresist (AZ 5214E) was spin coated on bare silicon substrate and soft baked. Then the silicon substrate was

exposed to UV beam topped by a photomask and reversal baking was processed. After second UV exposure without a photomask, the photoresist was developed by a developer solution (MIF 500). Using e-beam evaporator, 100 nm gold was deposited as a first metal layer. For the adhesion between substrate and gold, 3 nm- chromium was deposited priorly. To remove photoresist residual, sample was sonicated with acetone. A 30 nm layer of Al_2O_3 was grown on the surface of sample through atomic layer deposition (ALD) process. Subsequently, second metal deposition was conducted. The remnant second metal layer left on the first layer was tapped off. Lastly, sample was dipped in KOH solution for 30 seconds to etch Al2O3 out of the metal surface. The rectangular shaped- gap of 30 nm was formed with side lengths of 10 um and 40 um. The rectangular arrays occupied the whole area of substrate surface with the 20 um by 50 um periodicity. The microscope image of 30 nm-width-slot antenna is displayed in Fig. 7 (b).

4-2. THz-TDS setup

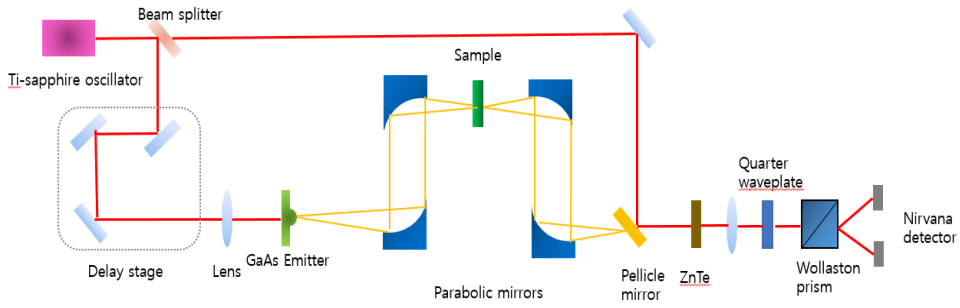

Figure 8 The scheme of terahertz time domain spectroscopy setup

We performed far-field THz time domain spectroscopy (THz-TDS). By measuring time domain signal, we can get both time and phase information of samples. Femtosecond pulses of 780 nm-center wavelength generated by Ti:sapphire mode locking were split by polarizing beam splitter for generation and detection THz signals. One of the infrared beam was focused onto a GaAs photoconductive antenna to generate a THz single pulse with maximum field strength of 30 V/cm and the other infrared beam was collected to ZnTe crystal to detect THz signal by electro optic sampling. The emitted THz pulse was focused on the sample by off-axis parabolic mirrors. The 1 um-width-slot antenna was aligned so that the short side of rectangular was parallel to the polarization of the pulse. For ring shaped-nanogap of 30 nm sample, the short side of rectangular shape was aligned in the same manner. To measure only 1mm by 1mm area of

samples, a thick aluminum plate with 1 mm by 1 mm square hole was attached to the sample on the incident side. The transmitted electric field in time domain data is computationally fourier transformed to get spectral amplitude and phase in a range from 0.2 THz to 1.5THz. Then, the far-field transmittance through the sample was normalized with the one through bare silicon substrate.

4-3. PEDOT:PSS drop casting

The aqueous PEDOT:PSS solutions of different concentration were prepared by diluting the pristine one with DI water. Pristine PEDOT:PSS aqueous solution, consisting of 1.3 wt.% PEDOT:PSS (weight ratio of PEDOT to PSS 1 : 1.6) dispersed in water was purchased from Sigma Aldrich, USA. The conductivity of pristine PEDOT:PSS was 1 S/cm. By diluting pristine solution with different amount of water, four additional solutions of 0.5 wt.%, 0.1 wt.%, 0.01 wt.%, 0.001 wt.% were obtained. Then, each of solution was stirred for 12 hours. 5 ul of each solution was drop casted on the slot antenna followed by baking of 120 degree for 10 mins.

To get more uniform polymer film on gold surface, dropped solution was confined in a rubber o-ring with inner diameter 5 mm. To avoid surface roughness caused by coffee ring effect, the area between center of circle and outermost area was chosen for the measurement. Drying of confined solution at room temperature followed by 120 degree baking could produce uniform area of 1 mm by 1 mm.

5. Results

5-1. Refractive index of PEDOT:PSS film

To get the refractive index of PEDOT:PSS, aqueous PEDOT:PSS solution of two different dilutions (0.5 wt.%, 1.3 wt.%) were drop casted on silicon substrate and after baking, THz transmission was measured. For the lower dilutions (0.1 wt.% , 0.01 wt.% and 0.001 wt.%), sample signal was barely distinguishable with the reference one. By considering Fabry-Perot effect, multiple reflections at interfaces of flat and parallel mediums, refractive index of polymer film can be deduced from the measured complex transmission coefficients (amplitude and phase). (37) The complex transmission coefficients is obtained by dividing the transmission signal with sample (F_{sample}) by the transmission signal without sample (F_{ref}). (The scheme shown in Fig. 9)

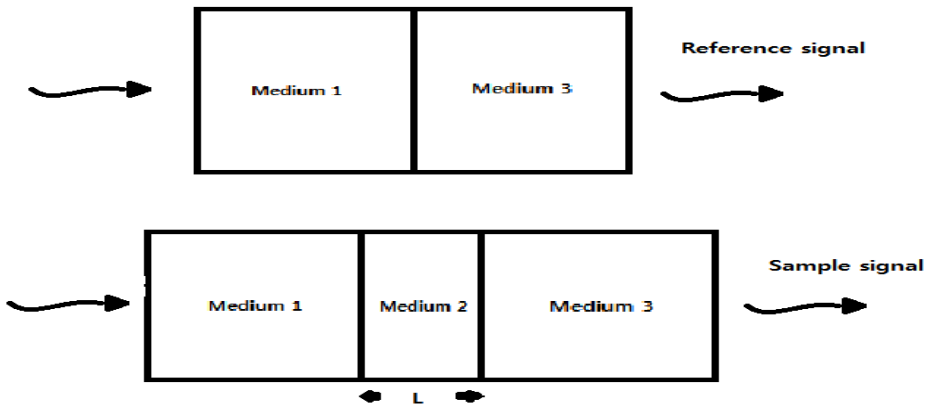

Figure 9 Scheme of medium arrangement for reference and sample signals

$$T_{sample}(\omega) = \frac{F_{sample}(\omega)}{F_{ref}(\omega)} = \frac{2\tilde{n}_2(\tilde{n}_1+\tilde{n}_3)}{(\tilde{n}_1+\tilde{n}_2)(\tilde{n}_2+\tilde{n}_3)} \times \exp[-j(\tilde{n}_2 - \tilde{n}_{air})\frac{\omega L}{c}] \times$$

$FP(\omega)$, where $FP(\omega)$ represents the Fabry-Perot term given by $FP(\omega) = \frac{1}{1-(\frac{\tilde{n}_2-\tilde{n}_1}{\tilde{n}_2-\tilde{n}_1})(\frac{\tilde{n}_2-\tilde{n}_3}{\tilde{n}_2-\tilde{n}_3})\times\exp[-2j\tilde{n}_2\frac{\omega L}{c}]}$

Here n, ω, c and L denote refractive index of each medium, angular frequency, velocity of light and thickness of sample film, respectively. In our case, air and silicon substrate were chosen as medium 1 and medium 3. The refractive index of silicon substrate, 3.53, was extracted from temporal delay between first and second pulse signal in time domain. The thickness of each polymer film was obtained by cross-sectional SEM (Scanning Electron Microscope) image. 750 nm and 3 um correspond to 0.5 wt.% and 1.3 wt.%, respectively. With the measured complex transmission, the unknown sample refractive index can be deduced using an algorithm called "on-the-downhill" method. (38) At the frequency of 0.5 THz and 0.75 THz, the resultant values are presented in Table 1.

Refractive index / Concentration	0.5 THz		0.75 THz	
	n	k	n	k
0.5 wt.%	18.42	9.02	15.56	7.56
1.3 wt.%	10.05	4.8	8.99	5.64

Table 1 Refractive index of PEDOT:PSS film of different concentration at 0.5 THz (left) and 0.75 THz (right)

As concentration is lowered, both real and imaginary part are increased, which implies higher conductivity. The morphology of PEDOT:PSS is that conductive PEDOT:PSS grains are surrounded by insulating shell of excess PSS chains. The conduction of PEDOT:PSS originates from hopping of charge carriers between the PEDOT-rich grains. (39, 40) Considering this fact, lower conductivity in thicker film is possibly attributed to the slight water remnant in between PEDOT:PSS grains, which interrupts hopping mechanism.

5-2. Transmission of slot antennas

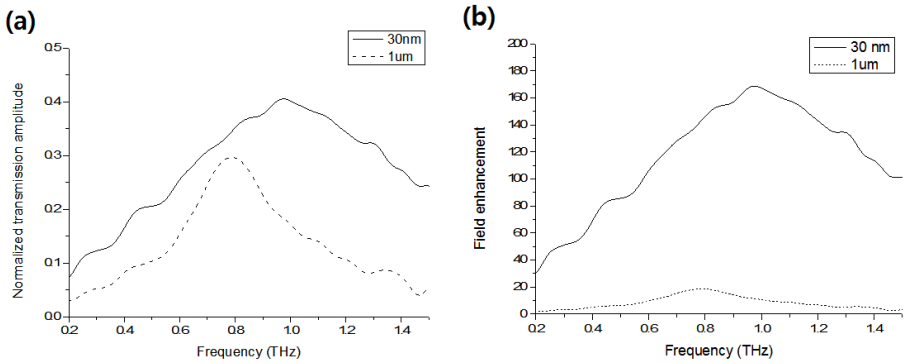

Figure 10 Transmission spectrum of slot antennas

The transmission amplitude and field enhancement are presented at Fig. 10. The transmission amplitude was normalized with the reference signal where the terahertz waves penetrate only the bare silicon substrate. The peak resonances are 0.98 THz and 0.78 THz for a 30 nm-sample and a 1 um-sample, respectively. In the far field detection scheme, field inside metal gap can be approximately obtained using Kirchhoff integral formalism. (41) According to this, field enhancement, the ratio of electric field inside gap to incident electric field, is simply obtained by dividing normalized amplitude by the coverage ratio of nanogaps to the whole sample. The field enhancement of 1 um-sample is 19. For 30 um-sample, the field enhancement was 169, approximately 9 folds higher than former one.

5-3. Transmission of PEDOT:PSS on slot antennas

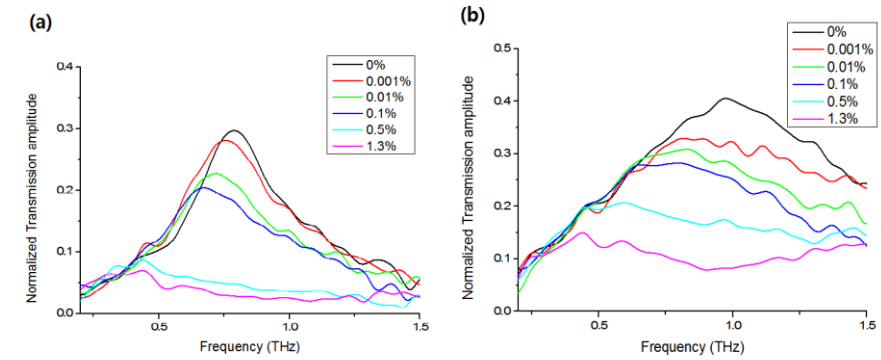

Figure 11 Transmission of slot antennas covered by each PEDOT:PSS solution (Left : 1 um-width slot, Right : 30 nm-width slot)

Fig. 11 (a) and (b) depict normalized transmission spectrum of 1 um (left) and 30 nm (right) sample respectively baked with solutions of various dilution. Since the conductivity value brings increment on both the real and imaginary part of refractive index, redshift of resonance and transmission decrease observed altogether.

Before further mention about the graph above, it is required to know about distribution of polymer around the metal gap. Regarding to the cross-sectional SEM image, polymer accumulated well inside the metal gap of 1 um width. However, for the 30 nm sample, considering the fact that the size of PEDOT:PSS

grain distributes from 20 nm to 80 nm (40), it may assumed that the polymer bridges over the metal gap.

In 0.001 % case, 30 nm sample displayed much higher transmission decrease than 1 um-width sample despite of different spatial distribution of polymer. The transmission decrease of 30 nm gap is 19 % which is more than 3 folds higher than the one of 1 um gap (5.7%).

In 0.01 % and 0.1 % cases, both samples displays similar extent of decrease in transmission despite of 1 order difference in field enhancement. In nano-gap case, the electric field decays away from gap surface and the spatial decay range is similar order with the gap width. (24) Considering that the thickness of 0.1 % polymer is 30 nm, there should be a lot more transmission decrease for 30 nm. It is inferred that the height mismatch between first and second metal layer rendered the decay range narrower. (42) Accordingly, the polymer distribution of further accumulation is not confined in strong-field region for 30 nm sample.

While the transmission decrease of 1 um sample is almost saturated after 0.5 % concentration, saturation was not observed for 30 nm sample until pristine one. In nanogap sample, it is expected that further accumulation of polymer brings additional gravity of polymer which plays closer contact between polymer and metal gap.

5-4. Analytic calculation of transmission of PEDOT:PSS on slot antennas

In this thesis, modal expansion method designed by Garcia-Vidal et al. (18) is incorporated as a tool for the analytic calculation of transmission of slot antennas. In this theory, PEC (perfect electric conductor) condition is assumed where the conductivity of metal is supposedly infinite. The electromagnetic field is expanded in k-space in the incident region (I) and in the transmission region (III). (See below in Fig. 12 (a))

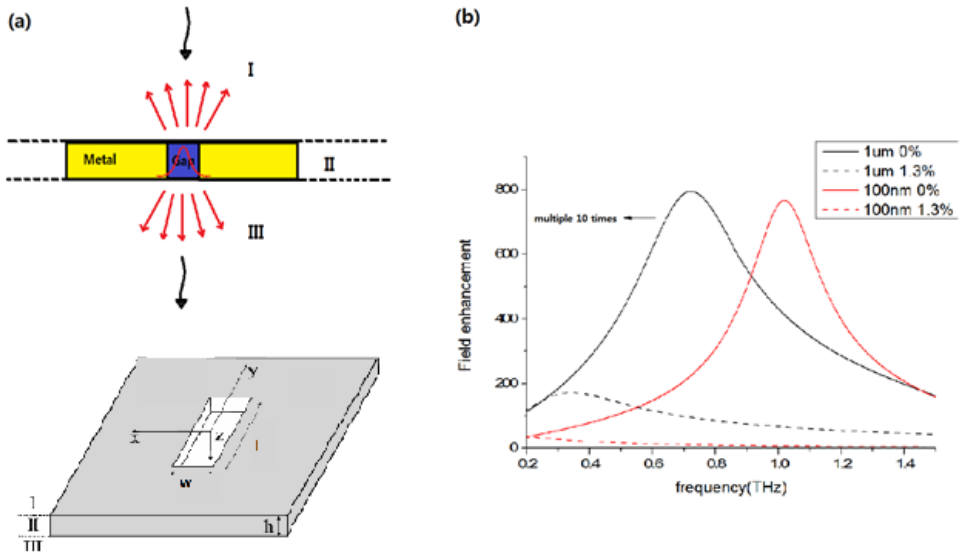

Figure 12 (a) The modal expansion scheme (b) Field enhancement of slot antennas (width: 1 um (black) and 100 nm (red)) with gap filled with air (straight line) or PEDOT:PSS (dot line)

Since the slot width is much smaller than the length as in our case, it is assumed that only a single mode of TE_{10} in the gap region (II) is excited by the incident field. The fields are written as below.

$$H_y^{\mathrm{I}} = \sqrt{\frac{\varepsilon_0}{\mu_0}} \int dk_x dk_y [\delta(k_x)\delta(k_y) e^{ik_{1z}z} + g_y(k_x, k_y) e^{i\theta} e^{-ik_{1z}z}]$$

$$H_y^{\mathrm{III}} = \sqrt{\frac{\varepsilon_0}{\mu_0}} \int dk_x dk_y [f_y(k_x, k_y) e^{i\theta} e^{ik_{3z}(z-h)}]$$

$E_x^{\mathrm{II}} = \cos\frac{\pi y}{l} [\mathrm{A} e^{i\beta z} + B e^{-i\beta z}]$, where $\beta = \sqrt{\varepsilon_2 k_0^2 - (\frac{\pi}{l})^2}, \theta = k_x x + k_y y.$

With continuous boundary conditions of electromagnetic fields at the interfaces between region I and region II and between region II and region III as expressed below,

$$H_y^{\mathrm{I}}(z=0) = H_y^{\mathrm{II}}(z=0)$$

$$E_x^{\mathrm{I}}(z=0) = E_x^{\mathrm{II}}(z=0)$$

$$H_y^{\mathrm{III}}(z=h) = H_y^{\mathrm{II}}(z=h)$$

$$E_x^{\mathrm{III}}(z=h) = E_x^{\mathrm{II}}(z=h)$$

we finally reach an equation for the electric field at the center of the gap exit,

$$E_{gap} = \frac{I_0 G_V}{(G^{\mathrm{I}} - \Sigma)(G^{\mathrm{III}} - \Sigma) - G_V^2}, \quad \text{where } \Sigma = \frac{\frac{\beta}{k_0}}{tan\beta\mathrm{h}}, \; G_V = \frac{\frac{\beta}{k_0}}{sin\beta\mathrm{h}}, \; I_0 = \frac{4\sqrt{2}}{\pi i},$$

$$G^{\text{I,III}} = \frac{i}{(2\pi)^2}\int dk_x dk_y \left[\frac{k_x^2+k_{1,3z}^2}{k_0 k_{1,3z}}\frac{wl}{2}\right]\left|\frac{2}{wl}\int_{gap\ area} dxdy cos\frac{\pi y}{l} e^{-i\,\theta}\right|^2$$

Lastly, as moving from a single slot case to a periodical slot arrays case, the k-space integrals are replaced with the summation of $\sum_m \frac{2\pi}{d} m$ where m is integer and d is the periodicity of array pattern.

Field enhancement was calculated for each case where the gap is filled with or without PEDOT:PSS. (See the Fig.12 (b)) The slot widths were chosen as 100 nm and 1 um. The other slot specifications are chosen same as the one of 1 um-width sample. The case of narrower width (less than 100 nm) was limited for the exact calculation with PEC condition. In this calculation, the real and imaginary part of refractive index of PEDOT:PSS were selected as 8.99 and 5.64 respectively corresponding to the values of 1.3 wt.% solution at 0.75 THz.

The transmission decrease of 1 um-width slot antenna was 78.2 % which was even higher than the experimental value, 76.4 % where the additional 3 um polymer accumulation brought further decrease in transmission. It is expected that the photoresist remnant inside the gap alleviated the transmission decrease. It is noticeable that the calculated transmission decrease in 100 nm-width case reaches 95.6 %. The highest experimental transmission decrease of 30 nm-width sample was 63.2 %. If the conductive polymer could well trapped inside the gap, a lot more decrease (more than 95.6 %) is achievable.

6. Summary

PEDOT:PSS has been actively and widely used for its superb properties such as processiblity, conductivity, compatibility and stability. In this thesis, diluted aqueous PEDOT:PSS solution was employed as a tool for the inspection of the effect of conductive polymer on transmission decrease of slot antennas.

Despite of 5 orders difference in conductivity between PEDOT:PSS and gold metal, noticeable change in transmission decrease was observed in both 1 um-width and 30 nm-width sample covered by nano sized polymer film. Especially, for the lowest concentration (0.001 wt.%), 30 nm sample performed approximately 3 folds higher sensitivity over 1 um sample. More drastic transmission decrease of nano gap can be achieved by geometric adjustment such as height match of metal layers, thinner metal layer and narrower gap.

The conductivity of PEDOT:PSS is affected by gas environment such as humidity, ammonia and carbon dioxide etc. (11, 43) Considering the ability of slot antennas to detect the nano-thin film in transmission, slot antenna can bring further improved sensitivity and faster response to the sensor devices. (39) The higher performance can be achieved with a narrower gap sample.

7. References

1. T.W.Ebbesen, H.J.Lezec, P.A Wolff, et al. Extraordinary optical transmission through sub-wavelength hole arrays. Nature. 1988; 391, 667-69

2. K. J. Klein Koerkamp, S. Enoch, F. B., L. Kuipers, et al. Strong Influence of Hole Shape on Extraordinary Transmission through Periodic Arrays of Subwavelength Holes. Phys. Rev. Lett. 2004; 92, 183901

3. Raether, Heinz. Surface Plasmons on Smooth and Rough Surfaces and on Gratings. 1988; Springer

4. William L. Barnes, Alain Dereux, Thomas W. Ebbesen. Nature. 2003; 424, 824-30

5. D. Gacemi, J.Manageney, R.Colombeli, et al. Subwavelength metallic waveguides as a tool for extreme confinement of THz surface waves. Scientific Reports. 2013; 3, 1369

6. M. A. Seo, H. R. Park, D. S. Kim, et al. Terahertz field enhancement by a metallic nano slit operating beyond the skin-depth limit. Nature. 2009; 3, 152-56

7. H.R.Park, K.J.Ahn, Dai-Sik Kim, et al. Colossal Absorption of Molecules Inside Single Terahertz Nanoantennas. Nano Lett. 2013; 13 (4), 1782−86

8. Dong-Kyu Lee, Ji-Hun Kang, Q-Han Park, et al. Highly sensitive and selective sugar detection by terahertz nano-antennas. Scientific Reports. 2015; 5, 15459

9. Dong-Kyu Lee, Ji-Hun Kang, Q-Han Park, et al. Nano metamaterials for ultrasensitive Terahertz biosensing Scientific Reports. 2017; 7, 8146

10. Minah Seo, Ji-Hun Kang, Q-Han Park, et al. Observation of terahertz-radiation-induced ionization in a single nano island. Scientific Reports. 2015; 5, 10280

11. Jin-Kwan Park, Tae-Gyu Kang, Hyang Hee Choi, et al. Real-time Humidity Sensor Based on Microwave Resonator Coupled with PEDOT:PSS Conducting Polymer Film. Scientific Reports. 2018; 8, 439

12. Christoph DrexlerTatiana V. Shishkanova, Vladimir M. Mirsky, et al. Terahertz split-ring metamaterials as transducers for chemical sensors based on conducting polymers: a feasibility study with sensing of acidic and basic gases using polyaniline chemosensitive layer, Microchimica Acta.. 2014; 181(15-16), 1857-62

13. F. J. García-Vidal, Esteban Moreno, L. Martín-Moreno, et al. Transmission of Light through a Single Rectangular Hole. Phys. Rev. Lett. 2005; 95, 103901

14. Xiaoshu Chen, Hyeong-Ryeol Park, Dai-Sik Kim, et al. Atomic layer lithography of wafer-scale nanogap arrays for extreme confinement of electromagnetic waves Nature Communications. 2013; 4, 2361

15. J. H. Kang, D. S. Kim, and Q-Han Park. Local Capacitor Model for Plasmonic Electric Field Enhancement. 2009; Phys. Rev. Lett. 102, 093906

16. Young-Mi Bahk, Sanghoon Han, Dai-Sik Kim, et al. Ultimate terahertz field enhancement of single nanoslots. Phys. Rev. B. 2017; 95, 075424

17. Dasom Kim, Jeeyoon Jeong, Dai-Sik Kim, et al. Giant Field Enhancements in Ultrathin Nanoslots above 1 Terahertz. ACS Photonics. 2018; 5 (5), 1885−90

18. F. J. García-Vidal, L. Martín-Moreno, R. Gordon, et al. Transmission of light through a single rectangular hole in a real metal. Phys. Rev. 2006; B 74, 153411

19. Joon-Yeon Kim, Bong Joo Kang, Dai-Sik Kim, et al. Tunnelling current-voltage characteristics of Angstrom gaps measured with terahertz time-domain spectroscopy. Scientific Reports. 2016; 6, 29103

20. Joon-Yeon Kim, Bong Joo Kang, Dai-Sik Kim. Terahertz Quantum Plasmonics of N**anosl**ot Antennas in Nonlinear Regime. Nano Lett. 2015; 15 (10), 6683−6688

21. J. H. Kang, Jong-Ho Choe, Q-Han Park. Substrate effect on aperture resonances in a thin metal film. Optics Express. 2009; 17 (18), 15652-58

22. Om Krishna Suwal, Jiyeah Rhie, Dai-Sik Kim. Nonresonant 104 Terahertz Field Enhancement with 5-nm Slits. Scientific Reports. 2017; 7, 45638

23. Mostafa Shalaby, Hannes Merbold, Hans Sigg, et al. Concurrent field enhancement and high transmission of THz radiation in nanoslit arrays. Appl. Phys. Lett. 2011; 99, 041110

24. Hyeong-Ryeol Park, Xiaoshu Chen, Sang-Hyun Oh, et al. Nanogap-Enhanced Terahertz Sensing of 1 nm Thick (λ/106) Dielectric Films. ACS Photonics. 2015; 2 (3), 417−24

25. Young-Gyun Jeong, Sanghoon Han, Dai-Sik Kim, et al. A Vanadium Dioxide Metamaterial Disengaged from Insulator-to-Metal Transition. Nano Lett. 2015; 15 (10), 6318−23

26. L. Groenendaal, F. Jonas D. Freitag, J. R. Reynolds, et al. Poly(3,4-ethylenedioxythiophene) and Its Derivatives: Past, Present, and Future. Advanced Materials. 2000; 12 (7) 481-94

27. Stephan Kirchmeyer and Knud Reutera. Scientific importance, properties and growing applications of poly(3,4-ethylenedioxythiophene). J. Mater. Chem. 2005; 15, 2077-88

28. Yijie Xia and Jianyong Ouyang. PEDOT:PSS films with significantly enhanced conductivities induced by preferential solvation with cosolvents and their application in polymer photovoltaic cells. J. Mater. Chem. 2011; 21, 4927-36

29. Yijie Xia,a Hongmei Zhanga and Jianyong Ouyang. Highly conductive PEDOT:PSS films prepared through a treatment with zwitterions and their application in polymer photovoltaic cells. J. Mater. Chem. 2010; 20, 9740-47

30. Zhengyou Zhu, Congcong Liu, Endou Liu, et al. Improving the electrical conductivity of PEDOT:PSS films by binary secondary doping. Electronic Materials Letters. 2016; 12 (1), 54-8

31. Zhimeng Yu, Yijie Xia, Jianyong Ouyang, et al. PEDOT:PSS Films with Metallic Conductivity through a Treatment with Common Organic Solutions of Organic Salts and Their Application as a Transparent Electrode of Polymer Solar Cells. Appl. Mater. Interfaces; 2016, 8 (18), 11629−38

32. Ziyang Hu, Jianjun Zhang, Ying Zhaoa, et al. Influence of doped PEDOT:PSS on the performance of polymer solar cells. Solar Energy Materials and Solar Cells. 2011; 95 (10), 2763-67

33. Natsumi Ikeda, Tomoyuki Koganezawa, Ken-ichi Saitow. Performance of Si/PEDOT:PSS Hybrid Solar Cell Controlled by PEDOT:PSS Film Nanostructure. J. Phys. Chem. C. 2016; 120 (34), 19043−48

34. M. M. de Kok, M. Buechel, V. van Elsbergen, et al. Modification of PEDOT:PSS as hole injection layer in polymer LEDs. Physics of Organic Semiconductors. 2004; 201(6), 1342-59

35. Chu-Jung Ko. Modified buffer layers for polymer photovoltaic devices. Appl. Phys. Lett. 2007; 90, 063509

36. Mourad Boussoualem, Roch Chan Yu King, Frédérick Roussel, et al. Electro-optic and dielectric properties of optical switching devices based on liquid crystal dispersions and driven by conducting polymer [poly(3,4-ethylene dioxythiophene):polystyrene sulfonate (PEDOT:PSS)]-coated electrodes. Journal of Applied Physics. 2010; 108, 113526

37. L. Duvillaret, F. Garet, J.-L. Coutaz. A reliable method for extraction of material parameters in terahertz time-domain spectroscopy Journal of Selected Topics in Quantum Electronics. 1996; 2 (3), 739-46

38. Da-xiang Zhou, E. P. J. Parrott, J. Axel Zeitler, et al. Determination of complex refractive index of thin metal films from terahertz time-domain spectroscopy. Journal of Applied Physics. 2008; 104, 053110

39. A.M. Nardes, On the conductivity of PEDOT:PSS thin films. Technische Universiteit Eindhoven. 2007

40. Vitoratos S. Sakkopoulosa, E. Dalasb, S. A. Choulisd. Correlation between Thickness, Conductivity and Thermal Degradation Mechanisms of PEDOT:PSS Films. AIP Conference Proceedings. 20110; 1203, 178

41. J.S.Kyoung, M.A.SeoH, D.S.Kim, et al. Far field detection of terahertz near field enhancement of sub-wavelength slits using Kirchhoff integral formalism Optics Communications, 2010; 283 (24), 4907-10

42. Sanghoon Han, Young-Mi Bahk, Dai-Sik Kim, et al. Terahertz field enhancement in asymmetric and tapered nano-gaps. Optics Express. 2016; 24 (3), 2065-71

43. Mahdieh Hakimi, Alireza Salehi and Farhad A. Boroumand. Fabrication and Characterization of an Ammonia Gas Sensor Based on PEDOT-PSS With N-Doped Graphene Quantum Dots Dopant. Sensors Journal. 2016; 16 (16), 6149-54

국 문 초 록

PEDOT : PSS 는 탁월한 가공성, 열 안정성, 유기적 호환성, 높은 전기적 전도성으로 인해 광전지, 태양 전지 및 센서와 같은 전기적, 광학적 장치에서의 응용에 활발히 연구되고 있다. 이 논문에서는 PEDOT : PSS 수용액을 마이크로에서 나노 크기까지의 폭을 가지는 각 슬롯 안테나 위에 희석량을 달리한 PEDOT : PSS 수용액 물방울을 떨어뜨려 말린 후, 테라헤르츠를 투과시켜, 테라헤르츠 투과율 측정하였다. PEDOT : PSS 는 안테나 구멍을 가로지르는 전류통로를 만들어 줌으로써, 전기용량적 전하 축적을 완화시키며, 따라서 테라헤르츠 투과율을 감소시킨다. PEDOT : PSS 의 전도도는 금속의 전도도보다 대략 10^5 배나 작음에도 불구하고, 안테나 구멍 내부의 강한 전기장의 도움을 받아, PEDOT : PSS 의 테라헤르츠 투과율 감소가 뚜렷이 측정이 되었다. 0.001 중량 %의 극도로 희석 된 PEDOT : PSS 수용액의 경우, 각각 30nm 및 1um 슬롯 안테나에 대해 19 % 및 5.7 %의 투과율 감소를 보였다. 이 결과는 PEDOT : PSS 의 얇은 박막이 실시간 가스 감지 디바이스에 향상된 감지능력을 가져올 것으로 전망된다.

주요어 : 테라헤르츠 투과도, PEDOT:PSS, 나노슬랏 안테나

학 번 : 2017-22335